

Theoretical study of the gas-phase Fe^+ -mediated oxidation of ethane by N_2O

Lianming Zhao · Wenyue Guo · Zhaochun Liu ·
Yuanyuan Li · Xiaoqing Lu

Received: 12 September 2010/Accepted: 29 November 2010/Published online: 24 December 2010
© Springer-Verlag 2010

Abstract We report herein a comprehensive study of the gas-phase Fe^+ -mediated oxidation of ethane by N_2O on both the sextet and quartet potential energy surfaces (PESs) using density functional theory. The geometries and energies of all the relevant stationary points are located. Initial oxygen-atom transfer from N_2O to iron yields FeO^+ . Then, ethane oxidation by the nascent oxide involves C–H activation forming the key intermediate of $(\text{C}_2\text{H}_5)\text{Fe}^+(\text{OH})$, which can either undergo C–O coupling to $\text{Fe}^+ + \text{ethanol}$ or experience β -H shift giving the energetically favorable product of $\text{FeC}_2\text{H}_4^+ + \text{H}_2\text{O}$. Reaction of FeC_2H_4^+ with another N_2O constitutes the third step of the oxidation. N_2O coordinates to FeC_2H_4^+ and gets activated by the metal ion to yield $(\text{C}_2\text{H}_4)\text{Fe}^+\text{O}(\text{N}_2)$. After releasing N_2 through the direct H abstraction and/or cyclization pathways, the system would be oxidized to ethenol, acetaldehyde, and oxirane, regenerating Fe^+ . Oxidation to acetaldehyde along the cyclization –C–to–C hydrogen shift pathway is the most energetically favored channel.

Electronic supplementary material The online version of this article (doi:[10.1007/s00214-010-0873-9](https://doi.org/10.1007/s00214-010-0873-9)) contains supplementary material, which is available to authorized users.

L. Zhao (✉) · W. Guo (✉) · Z. Liu · Y. Li
College of Physics Science and Technology,
China University of Petroleum, Dongying,
Shandong 257061, People's Republic of China
e-mail: lmzhao@upc.edu.cn

W. Guo
e-mail: wyguo@upc.edu.cn

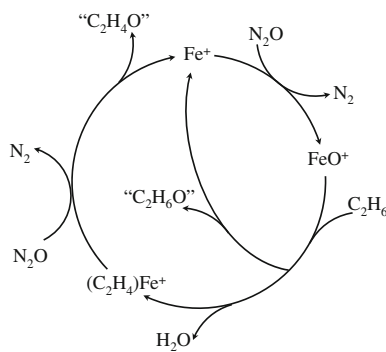
X. Lu
Department of Physics and Materials Science,
City University of Hong Kong, Hong Kong SAR,
People's Republic of China

Keywords Gas phase · DFT · Oxidation · PES

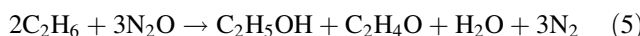
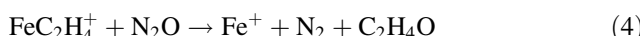
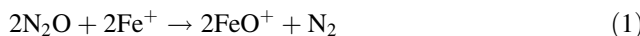
1 Introduction

Selective oxidation of hydrocarbons catalyzed by transition metals is of fundamental importance in various branches of chemistry, biology, and chemical engineering [1–10]. In this respect, gas-phase experiments combined with theoretical works have provided a wealth of information of elementary steps and intermediates for various catalytic reactions [3, 11, 12]. As the simplest hydrocarbon model containing a single C–C bond, ethane oxidation mediated by transition metal ions and their oxides has been experimentally extensively investigated [4, 11–20]. It was found that none of the M^+ ions ($M = \text{Cr–Ni}$) activates ethane at thermal energies, but under the same reaction conditions, all the corresponding MO^+ ions can activate the C–H bond of ethane and give the subsequent losses of ethanol, ethylene, and/or water [13, 15–18].

Owing to the low N_2 -oxygen affinity ($\text{OA}(\text{N}_2) = 40$ kcal/mol [19]), N_2O usually acts as a useful oxidant for the oxidation of organic compounds. In the gas-phase oxidation of ethane by N_2O , however, only Fe^+ presents high reactivity among all 3d transition-metal ions [3, 4, 20]. For the Fe^+ -mediated $\text{C}_2\text{H}_6/\text{N}_2\text{O}$ reaction cycle (reactions 1–5, see Scheme 1), initial O-atom transfer from N_2O to the metal ion affords the corresponding FeO^+ species (reaction 1) [20]. Then, the ethane oxidation by FeO^+ in part directly regenerates Fe^+ via liberating ethanol (reaction 2) but also mainly eliminates water producing FeC_2H_4^+ (reaction 3). Finally, the reaction cycle is complete via the further reaction of FeC_2H_4^+ with another N_2O to regenerate Fe^+ (reaction 4) [20].



Scheme 1 Reaction cycle for the Fe^+ -mediated oxidation of ethane by N_2O (Ref. [20])



For the sake of unveiling the reaction mechanisms, extensive theoretical studies on the reactions of ethane with Fe^+ , Co^+ , and other transition metal ions have been reported [21–25]. However, to our knowledge, electronic structure calculations of hydrocarbon oxidation by corresponding metal oxide ions are still mainly limited to methane, propane, and several other organic substrates, but rather scarce for ethane [26–46]. The oxidation of methane to methanol by all 3d transition-metal oxide ions was reported to occur via a direct H abstraction followed by methyl migration [26–30]. We also found the reaction of FeO^+ with propane involves initial C–H activation, and the products ($\text{C}_3\text{H}_7\text{OH}$, C_3H_6 , CH_3 , and H_2O) are in relation to the encounter complexes and spin inversion [32].

In comparison with the facts that FeO^+ brings about activation of methane with quite low efficiency and FeO^+ reaction with propane involves both C–C and C–H activation, FeO^+ was found to activate C–H bond in ethane efficiently at thermal energies [4, 15, 20, 47]. Hence, a theoretical study of the $\text{FeO}^+/\text{C}_2\text{H}_6$ reaction is needed to systematically understand the reactivity of FeO^+ toward hydrocarbons with different alkyl chains. In this article, we reported a comprehensive theoretical investigation of the Fe^+ -mediated oxidation of ethane by N_2O . One interesting reason for this study is iron oxide ion was found to present a good activity toward the inert saturated hydrocarbons both experimentally and theoretically [3, 11, 20, 26–30]. Second, the title reaction represents one of the prototype systems for the transition metal ion–mediated oxidation of the saturated hydrocarbons by N_2O . Third, the reaction of $\text{FeC}_2\text{H}_4^+/\text{N}_2\text{O}$ involved in the system associates with the

competitions of C–H and C–C activation vs. oxygen-atom transfer and carbonylation vs. epoxidation, which provides an efficient window to probe the selectivity for alkenes oxidation. Our main aim is to elucidate the reaction mechanisms and determine the activation barriers useful to give insight into kinetic aspects. This includes a complete description of all possible pathways on both the sextet and quartet PESs for the full oxidation process.

2 Computational details

All computations were carried out using the GAUSSIAN 03 program package [48]. Geometry optimizations and frequency calculations were carried out for all the relevant species using the hybrid density functional B3LYP [49–53] method together with the DZVP(opt + 3f) [31–34, 55] for Fe^+ and 6-311 ++G(2d, 2p) basis set [54] for the non-metal atoms. Our recent work has shown the performance of this computational strategy for describing the features of the PESs of the $\text{Fe}^+/\text{N}_2\text{O}/\text{hydrocarbon}$ systems [31, 32].

Intrinsic reaction coordinate (IRC) calculations were performed to identify the pathways between transition states and their connecting minima. The calculation method STABLE [56, 57] was used everywhere to ensure there were no instabilities in the wavefunction of stationary points. Natural bond orbital (NBO) [58–60] analyses were carried out to characterize the bonds and interactions inside some important complexes.

3 Results and discussion

In the following sections, we first establish the accuracy that is expected from the chosen level of theory for the $\text{Fe}^+/\text{N}_2\text{O}/\text{C}_2\text{H}_6$ system. Then, we examine the title reaction in detail, including the geometries of various stationary points and PESs for all the oxidation processes. Finally, we briefly compare our theoretical results with the experimental findings [15, 17, 20]. For simplicity, calculated total energies, zero-point energies as well as $\langle S^2 \rangle$ values for all the species involved are given as Supporting Information (see Table S1).

3.1 Calibration

To evaluate the reliability of the level of theory employed, we compare the experimentally thermochemical data with the results from our theoretical approach. Table 1 collects the theoretically predicted adiabatic bond dissociation energies (BDEs) and the most reliable experimental data for some relevant species [62–68]. As shown in Table 1, although the difference of the calculated excitation energy of $\text{Fe}^+ ({}^4\text{F}, 3\text{d}^7 \leftarrow {}^6\text{D}, 3\text{d}^6 4\text{s}^1)$ with the experimental gap

Table 1 Adiabatic bond dissociation energies and excitation energies (kcal/mol) at 0 K determined by calculations and experiments

Species	Calcd ^{a,b}	Expt
⁶ [Fe ⁺ -O]	76.9 (-3.1 ± 1.4)	80.0 ± 1.4^c
⁴ [Fe ⁺ -OH ₂]	29.7 (-0.9 ± 1.2)	30.6 ± 1.2^d
⁵ [Fe ⁺ -OH]	82.8 (0.2 ± 4)	82.6 ± 4^e
⁴ [Fe ⁺ -CO]	33.4 (2.1 ± 1.8)	31.3 ± 1.8^f
⁴ [Fe ⁺ -CH ₂]	77.8 (-3.7 ± 1.0)	81.5 ± 1.0^g
⁴ [Fe ⁺ -OCH ₂]	33.9 (1.0 ± 1.6)	$32.9. \pm 1.6^h$
⁴ [Fe ⁺ -N ₂]	13.4 (0.7 ± 0.9)	12.7 ± 0.9^i
⁴ [Fe ⁺ -C ₂ H ₄]	45.5 (10.9 ± 2.5)	34.6 ± 2.5^j
Fe ⁺ (${}^4F \leftarrow {}^6D$)	12.5 (6.7)	5.8 ^k

^a At the B3LYP/DZVP(opt + 3f):6-311 + G(2d,2p) level

^b Values in the parentheses are error bars for the calculated BDEs, obtained by subtracting the experimental values from the calculated BDEs

^c Ref. [61]

^d Ref. [62]

^e Ref. [63]

^f Ref. [64]

^g Ref [65]

^h Ref. [63]

ⁱ Ref. [66]

^j Ref. [67]

^k Ref. [68]

value is not small (12.5 vs. 5.8 kcal/mol [68]), the error of the calculated stability of both electronic states should be maintained during the overall reaction. Thus, the relative energies on the reaction energy profile should not be highly modified. It is also found from Table 1 that the calculations reproduce the experimental adiabatic BDEs well in most cases with the exception of ⁴[Fe⁺-C₂H₄]. Our calculated binding of ⁴[Fe⁺-C₂H₄] is overestimated by 10.9 kcal/mol, similar to the situation of the calculations by Holthausen et al. (52 kcal/mol at the B3LYP/Wachters: D95** level [23]) and Zhang et al. (41.6 kcal/mol at the B3LYP/6-311 ++G(3df,3pd)//B3LYP/6-311 + G** level [69]). The error may be as a systematic shortcoming of the B3LYP functional in the description of weakly bound complexes [23].

Due to the overbinding of ⁴[Fe⁺-C₂H₄], the relative stability of the FeC₂H₄⁺ + N₂O asymptote with respect to the remainder of the PES of the FeC₂H₄⁺/N₂O system is probably overestimated by 11 kcal/mol. However, the relative energies of the other parts of the PES are still described more satisfactorily. This is similar to the situation of the Fe⁺/C₂H₆ system reported by Holthausen et al. [23]. The present shortcoming to some extent limits the predictive power in quantitative terms; nevertheless, we are confident that the approach employed describes correctly the qualitative features of the PES.

3.2 N₂O reduction mediated by Fe⁺

The first step of the Fe⁺-mediated oxidation of ethane is the reaction between Fe⁺ and N₂O producing FeO⁺, which has been studied by us at the same level of theory [31]. Briefly, we found that FeO⁺ is generated via a direct O-abstraction mechanism on the sextet PES, whereas on the quartet pathway, a N–O insertion mechanism is favored. Considering the two-state reactivity phenomenon, the rate-limiting barrier for the N₂O reduction is located at 2.8 kcal/mol below the sextet entrance channel; and the overall reaction is exothermic by 35.9 kcal/mol.

3.3 C₂H₆ oxidation by FeO⁺

PES together with schematic structures involved is shown in Figs. 1 and 2. Information about the relevant species is given in Fig. S1 (Supporting Information). Ethane oxidation by FeO⁺ starts with the association of FeO⁺ with C₂H₆ forming two types of encounter complexes, i.e., **1a** and **1b**. Complexes **1a** and **1b** are characterized as η^3 -OFe⁺-C₂H₆, in which FeO⁺ via Fe⁺ is simultaneously coordinated with 2 α , β -, and 3 α -H atoms with the adiabatic binding energies of 29.8 (26.7) and 28.8 (23.4) kcal/mol in the sextet (quartet) state, respectively. As expected, the bindings are 6–7 kcal/mol stronger than OFe⁺-CH₄ (22.8 (16.4) kcal/mol at the B3LYP/Wachters:6-311G** level [27, 28]) but 8–10 kcal/mol weaker than OFe⁺-C₃H₈ (36.7 (33.6) kcal/mol at the same theoretical level [32]). The stability of OFe⁺-alkanes depends strongly on their structures, i.e., the η^2 -CH₄ complex [27, 28] accounts for the weakest binding, while the η^4 -C₃H₈ complex [32] affords the strongest binding. The difference in stabilities of complexes can be explained by electron transfers between FeO⁺ and the adjacent nucleophilic σ bonds in alkanes. NBO analysis shows that the association of OFe⁺-alkane favors strong electron donation from the adjacent σ (C–H) and σ (C–C) orbitals of alkanes to FeO⁺, suggesting that the number of adjacent σ bonds in alkanes is an important factor in determining the stability of OFe⁺-alkanes. This is perfectly consistent with the stability sequence as mentioned previously.

Through a direct C²-to-O H-shift, both **1a** and **1b** could give birth to hydroxyl complex (C₂H₅)Fe⁺(OH) (**2**), which lies at -51.2 (-56.6) kcal/mol in its sextet (quartet) state. The relevant transition states (**TS_{1a-2}** and **TS_{1b-2}**) lie at -7.1 (-12.6) and -3.9 (-7.0) kcal/mol, respectively, on the sextet (quartet) PES, suggesting a PESs crossing occurs before the transition state. Along the sextet coordinate, we also find a stepwise H-shift process from **1a** involving a (C₂H₅)Fe⁺H(O) minimum to **2** (See Fig. S2, Supporting Information). However, this path seems unlikely because it is located highly on the PES ($E_{\text{rel}} = \sim 16$ kcal/mol).

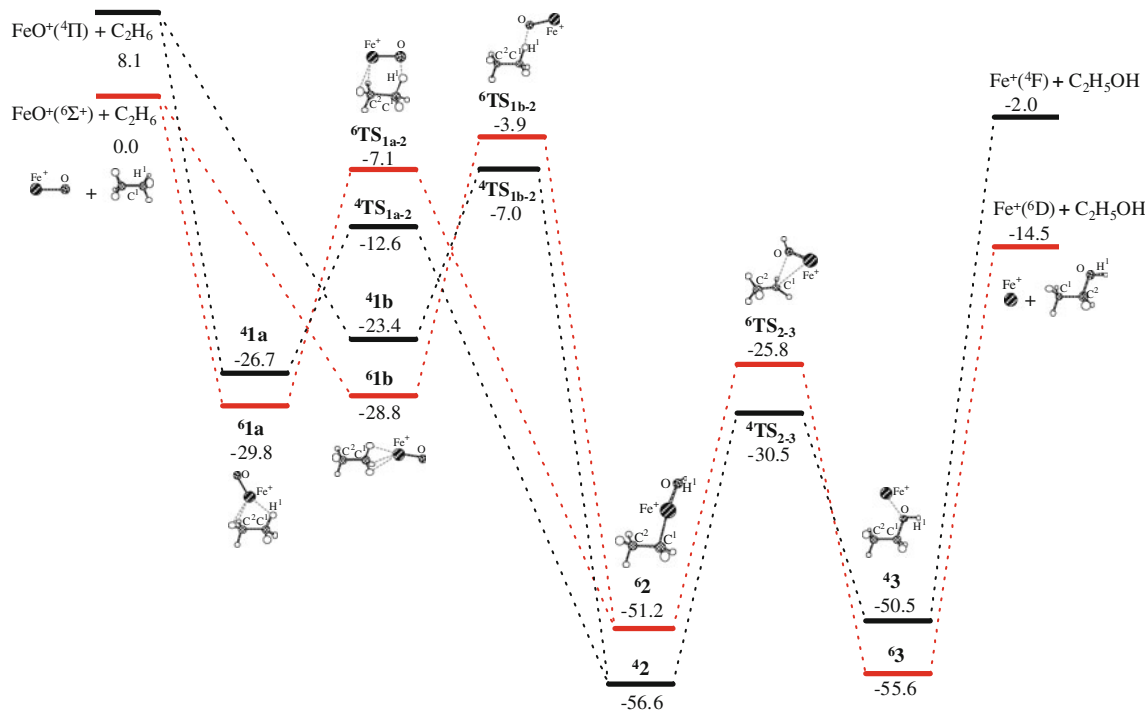
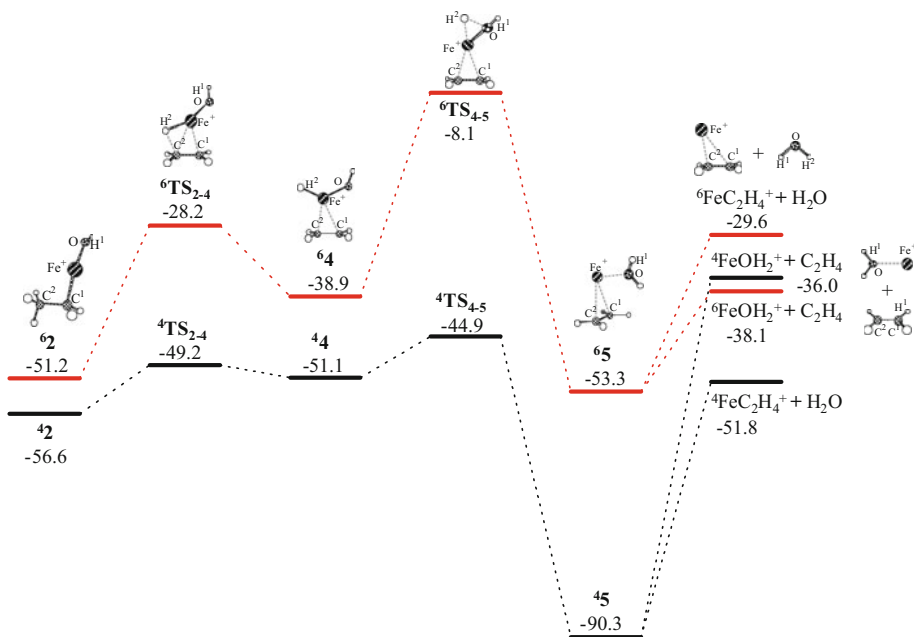


Fig. 1 Energy profile for the loss of ethanol involved in the C_2H_6 oxidation by FeO^+ . Numbers refer to the relative stabilities (kcal/mol) with respect to the reactants of $\text{C}_2\text{H}_6 + \text{FeO}^+(\text{6}\Sigma^+)$ evaluated at the

B3LYP/DZVP(opt + 3f):6-311 + G(2d,2p) level including ZPE corrections. Scaling factor for the ZPE is 0.961

Fig. 2 Energy profile for the losses of ethylene and water from complex $(\text{C}_2\text{H}_5)\text{Fe}^+(\text{OH})$ involved in the C_2H_6 oxidation by FeO^+ . Parameters follow the same notation as in Fig. 1



As shown in Fig. 1, one exit of species **2** is the subsequent coupling of the two end ligands to yield the $\text{Fe}^+(\text{ethanol})$ adduct (**3**), in which the metal attaches to the O atom of $\text{C}_2\text{H}_5\text{OH}$ with the Fe^+-O distance being 2.058 (1.980) Å for the sextet (quartet) state (see Fig. S1, Supporting Information). The new species is favored by the

high-spin state as its ground state (excitation energy of ${}^6\text{3} \rightarrow {}^4\text{3}$: 5.1 kcal/mol) rather than the reverse order as for its direct precursor **2**. The relevant transition state ${}^6\text{TS}_{2-3}$ ($E_{\text{rel}} = -25.8$ kcal/mol) lies above the quartet one by 4.7 kcal/mol, indicating a PESs crossing occurs after the transition state. Direct dissociation of Fe^+ -ethanol accounts

for the loss of ethanol and $\text{Fe}^+(\text{^6D or } \text{^4F})$, with the overall exothermicity of 14.5 or 2.0 kcal/mol.

In the actual oxidation of ethane by FeO^+ , ethanol elimination corresponds to only a branching ratio of 10–12% [15, 20]. Thus, the major part of species **2** undergoes β -H shift to form $(\text{C}_2\text{H}_4)\text{Fe}^+(\text{OH}_2)$ (**5**), the direct precursor of water- and ethylene-loss products (see Fig. 2). Different from the situation of **1a** \rightarrow **2**, this process involves stepwise metal-mediated β -H shift (**2** \rightarrow **4** \rightarrow **5**). As shown in Fig. 2, the sextet β -H shift branch occurs via high-energy barriers **TS₂₋₄** and **TS₄₋₅** ($E_{\text{rel}} = -28.2$ and -8.1 kcal/mol), while the quartet process involves a low-energy pathway with the highest barrier located at -44.9 kcal/mol (**TS₄₋₅**). In both states, species **5** can be explained as the dicoordination of metal center with the difference that Fe^+OH_2 and FeC_2 unit are co-plane and the Fe^+O bond is along the C_2 axis in the quartet (C_{2v}), whereas the sextet association (C_s) favors an out-of-plane location of the Fe^+O bond (the dihedral angle of Fe^+O to the FeC_2 -unit plane is 97.4°). NBO analysis suggests that the binding of Fe^+ with both the C_2H_4 and H_2O groups in **5** is dominated by electrostatic interaction as well as weak donor–acceptor stabilization due to the single occupation of the diffuse 4 s orbital of the metal. In the quartet, the relatively short distances between Fe^+ and ligands (see Fig. S1, Supporting Information) and the relatively strong stability of the species (lying at -90.3 kcal/mol or being 37.0 kcal/mol more stable than **5**) are caused by the much strong electron transfer ($\Delta E^{(2)} = 192.6$ kcal/mol). Indeed, the quartet species constitutes the deepest energy well on the whole PES. Different bond cleavage of ethylene- Fe^+ -water (**5**) accounts for products $\text{FeC}_2\text{H}_4^+ + \text{H}_2\text{O}$ and $\text{FeOH}_2^+ + \text{C}_2\text{H}_4$, with the overall exothermicities of 29.6 (51.8) and 38.1 (36.0) kcal/mol on the sextet (quartet) PES, respectively.

An overlook of the PESs of FeO^+ /methane [27, 28], ethane, and propane [32] shows that all the neutral products' eliminations start with initial C–H activation (C-to–O H-shift) forming the key intermediate (alkyl) $\text{Fe}^+(\text{OH})$, which is followed by three possible pathways, i.e., C–O coupling accounting for the common products, alcohols; Fe^+ -mediated alkyl H-shift for yielding water and alkenes in the $\text{FeO}^+/\text{C}_2\text{H}_6$ and C_3H_8 systems; and CH₃-shift for producing methyl in the $\text{FeO}^+ + \text{C}_3\text{H}_8$ reaction. The initial C–H activation with a sextet-to-quartet spin inversion constitutes the rate-determining step for all the three oxidation reactions. Considering the crossing of the PESs, ethane and propane experience almost same barriers to activate their C–H activation (17.2 v.s. 17.7 kcal/mol [32]), whereas the barrier for methane is slightly higher (22.1 kcal/mol [27, 28]). However, because the stability of $\text{FeO}^+(\text{alkane})$ increases gradually with the alkyl chain length as discussed previously, the C–H activation barriers

for $\text{C}_n\text{H}_{2n+2}$ ($n = 1–3$) are, respectively, 0.7 [27, 28], 12.6, and 19.0 [32] kcal/mol below the corresponding separated reactants ($\text{FeO}^+(\text{^6}\Sigma^+) + \text{alkane}$), and the reaction inclination favors the order of $\text{CH}_4 < \text{C}_2\text{H}_6 < \text{C}_3\text{H}_8$. This is in line with the experimental results ($k(\text{CH}_4) = (7.4 \pm 2.2) \times 10^{-10}$ cm³/molecule·s; $k(\text{C}_2\text{H}_6) = 8.4 \times 10^{-10}$ cm³/molecule·s at room temperature [20, 47, 70]).

3.4 FeC_2H_4^+ oxidation by N_2O

FeC_2H_4^+ oxidation by N_2O could result in five parallel neutral eliminations corresponding to H_2O , CH_4 , CH_2O , CH_2CH , and $\text{C}_2\text{H}_4\text{O}$ [20]. In the following, all possible mechanisms for these products are considered.

3.4.1 N_2O reduction by FeC_2H_4^+

PES together with the schematic structures involved is shown in Fig. 3. Information about the relevant species is given in Fig. S3 (Supporting Information). Initially, N_2O association with FeC_2H_4^+ yields $(\text{C}_2\text{H}_4)\text{Fe}^+(\text{N}_2\text{O})$ (**6**) stabilizing the system by 10.1 (22.3) kcal/mol in the sextet (quartet) state. Then, the system evolves into $(\text{C}_2\text{H}_4)\text{Fe}^+\text{O}(\text{N}_2)$ (**7**) through transition-state **TS₆₋₇** that lies at 19.4 (sextet) and -1.4 (quartet) kcal/mol. Because of the relatively weak interaction between the metal and N_2 , direct ejection of N_2 from species **7** finally gives $(\text{C}_2\text{H}_4)\text{Fe}^+\text{O}$ (**8**), which is nearly energetically degenerated in the high- and low-spin states (-34.5 and -34.3 kcal/mol).

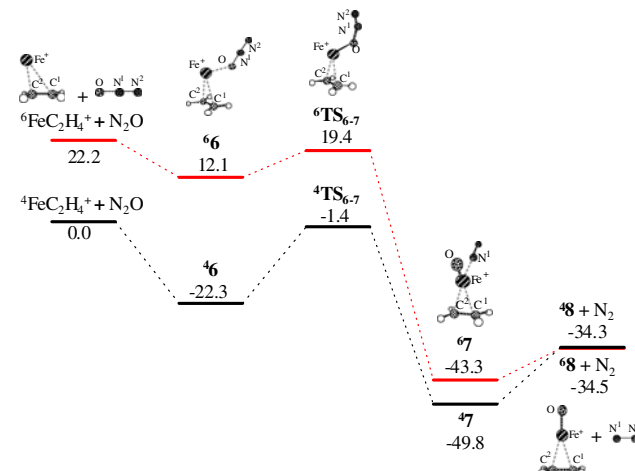


Fig. 3 Energy profile for N_2O reduction by FeC_2H_4^+ involved in the FeC_2H_4^+ oxidation by N_2O . Numbers refer to the relative stabilities (kcal/mol) with respect to the reactants of ${}^4\text{FeC}_2\text{H}_4^+ + \text{N}_2\text{O}$ evaluated at the B3LYP/DZVP(opt + 3f):6-311 + G(2d,2p) level including ZPE corrections. Scaling factor for the ZPE is 0.961

3.4.2 Regeneration of Fe^+

Using the internal energy acquired, species **8** could regenerate Fe^+ affording oxirane, acetaldehyde, and/or ethanol via direct H-abstraction and/or cyclization mechanisms. PESs together with the schematic structures involved are shown in Figs. 4 and 5. The information about the relevant geometries is given as Supporting Information (see Figs. S4 and S6).

(a) *Loss of oxirane and acetaldehyde.* Loss of oxirane and acetaldehyde is found to occur through the cyclization

mechanism. From Fig. 4, we can find that the mechanism implies an intramolecular rearrangement of FeO^+ in species **8** forming a “metallaaoxacyclobutane” species (**9**), which lies at -28.2 (-34.4) kcal/mol in its sextet (quartet) state. This process is expected to take place readily, because the relevant activation energy is only 15.6 (7.0) kcal/mol on the sextet (quartet) PES.

Species **9** conversion to the $\text{Fe}^+(\text{oxirane})$ adduct (**10**) involves different pathways on the different PESs, that is, the direct coupling of the metal-coordinated O and C atoms mediated by an $\text{O}-\text{C}^1-\text{C}^2$ scissor vibration along the

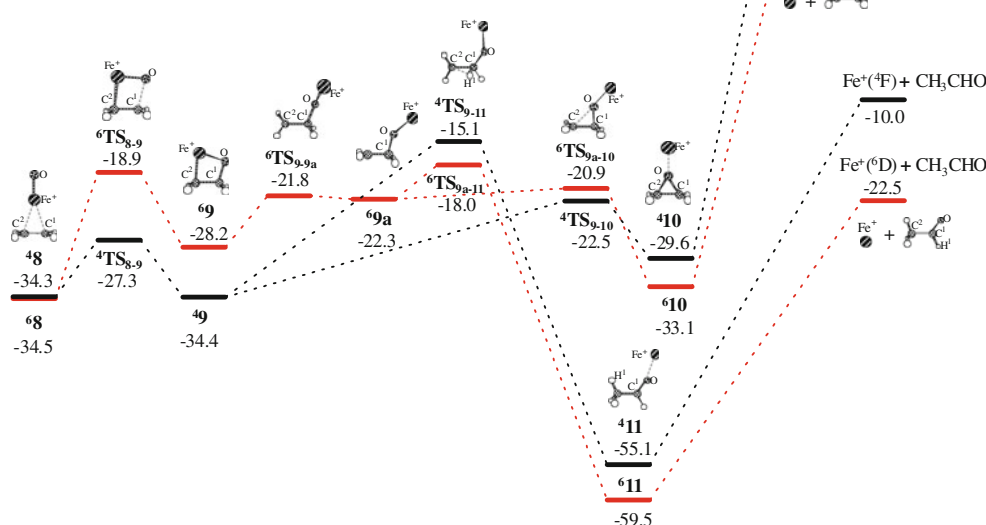
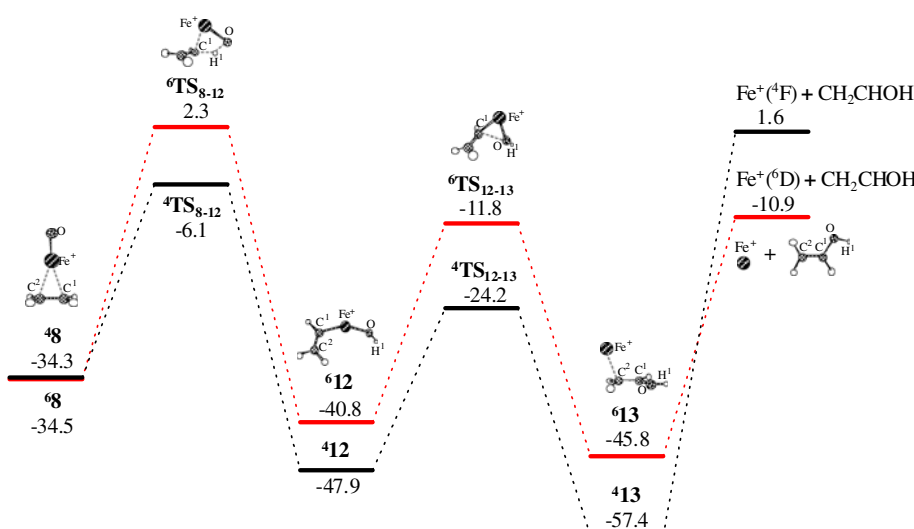


Fig. 4 Energy profile for the losses of acetaldehyde and oxirane via the cyclization mechanism involved in the FeC_2H_4^+ oxidation by N_2O . The ejected N_2 is not shown. Parameters follow the same notation as in Fig. 3

Fig. 5 Energy profile for the loss of ethanol via the direct hydrogen abstraction mechanism involved in the FeC_2H_4^+ oxidation by N_2O . The ejected N_2 is not shown. Parameters follow the same notation as in Fig. 3



quartet coordinate and the two-step reaction profile of homolytic ring-opening to $\text{Fe}^+\text{OCH}_2\text{CH}_2$ (**9a**) and subsequent C²-O coupling on the sextet PES. The sextet stationary points (⁶TS_{9-a}, ⁶TS_{9a-10}, and ⁶9a) are located in a flat region of –20.9 to –22.3 kcal/mol, slightly higher than the quartet barrier ⁴TS₉₋₁₀ ($E_{\text{rel}} = -22.5$ kcal/mol). Direct rupture of Fe^+ -oxirane (**10**) accounts for $\text{Fe}^+(\text{⁶D or } \text{⁴F}) + \text{oxirane}$, which is endothermic by 7.5 kcal/mol or located at 19.9 kcal/mol with respect to the reactants of $\text{FeC}_2\text{H}_4^+ + \text{N}_2\text{O}$.

Alternatively, direct C-to-C H-shift from species ⁶9a and ⁴9 yields the $\text{Fe}^+(\text{acetaldehyde})$ adduct (**11**). The new adduct is very stable, lying at –59.5 and –55.1 kcal/mol in its sextet and quartet states, and the relevant saddle points ⁶TS_{9a-11} and ⁴TS₉₋₁₁ are located at –18.0 and –15.1 kcal/mol, respectively. Direct decomposition of Fe^+ -acetaldehyde affords $\text{Fe}^+(\text{⁶D or } \text{⁴F})$ and acetaldehyde, with the overall exothermicity of 22.5 or 10.0 kcal/mol. Furthermore, the ⁶9a (⁴9) → **11** conversion could also proceed via Fe^+ -mediated H-transfer (see Fig. S5, Supporting Information), but it is less kinetically favorable due to the higher barrier as well as the more complex process involved.

(b) *Loss of ethanol.* Loss of ethenol is found to proceed via cyclization and/or direct H-abstraction mechanisms. The former involves metallacycle species **9** and then experiences a direct C²-to-O H shift yielding $\text{Fe}^+(\text{ethenol})$ adduct (**13**), which is assisted by the stretch of the Fe^+O bond (see Fig. S7, Supporting Information). However, the H-shift process needs to overcome a high-energy barrier (~6 kcal/mol above the energetic zero) and thus is kinetically unfavorable.

Alternatively, the direct H-abstraction mechanism offers a relative low-energy pathway. From Fig. 5, we can find that it occurs through direct C-to-O H shift from species **8** to form hydroxyl complex **12**, followed by a subsequent OH rebound yielding adduct **13**, with the H-shift barrier (**TS₈₋₁₂**) as the rate-determining point ($E_{\text{rel}} = 2.3$ (–6.1) kcal/mol for the sextet (quartet)). An obvious feature of adduct ⁶**13** is the attachment of the metal to the terminal C atom of CH_2CHOH , whereas the quartet counterpart favors a $\text{Fe}^+\text{-C}^1\text{-C}^2$ triangle structure. Such a situation has also been found for the $\text{Fe}^+(\text{ethynol})$ association [31]. The stability of the quartet state (lying at –57.4 kcal/mol or being 11.6 kcal/mol more stable than ⁶**13**) suggests that the triangle-type bonding stabilizes the species largely. Direct dissociation of Fe^+ -ethenol accounts for $\text{Fe}^+(\text{⁶D or } \text{⁴F}) + \text{ethenol}$, with the overall exothermicity of 10.9 or –1.6 kcal/mol.

Here, we make an inspection of the O-atom transfer PESs of $\text{OFe}^+(\text{C}_2\text{H}_4)$ and $\text{OFe}^+(\text{C}_2\text{H}_2)$ obtained at the same level of theory by us [31], which can be seen as the prototype of the oxidation of unsaturated hydrocarbons by late transition metal oxide ions. For both the ethylene and

acetylene oxidation by FeO^+ , the O-atom transfer product ($\text{C}_2\text{H}_4\text{O}/\text{C}_2\text{H}_2\text{O}$) could be carbonyl compound (acetaldehyde/ketene), hydroxy compound (ethenol/ethynol), and epoxy compound (oxirane/formylcarbene). From the point of view of applications, O-atom transfer to yield epoxides is one of the most important oxidation reactions of alkenes [4, 71]. However, although the oxirane formation experiences a simple cyclization and O-C coupling process, it is the least thermodynamically favorable due to the strong endothermicity, similar to the situation of formylcarbene. On the other hand, carbonylation (for acetaldehyde/ketene) is the most thermodynamically and kinetically favorable channel because of the strong exothermicity as well as low transition states along the production pathway (cyclization -C-to-C hydrogen shift). Hydroxylation (for ethanol/ethynol) as an energetically less-favorable oxidation channel proceeds according to direct H-abstraction and C–O coupling mechanism.

3.4.3 Formation of FeX^+ ($X = \text{CO}, \text{OH}, \text{C}_2\text{H}_2$, and CH_2)

We have extensively surveyed all possible pathways for the formation of by-products FeX^+ ($X = \text{CO}, \text{OH}, \text{C}_2\text{H}_2$, and CH_2). It is found that yielding FeCO^+ from $\text{Fe}^+(\text{acetaldehyde})$ (**11**) is too complex to compete with the direct CH_3CHO -loss channel (see Fig. S5, Supporting Information), explaining the minor FeX^+ (<12%) observed by the Fourier transform ion cyclotron resonance (FTICR) experiment [20]. Interestingly, we found the water-loss channel yielding FeC_2H_2^+ is exothermic by 30.7 kcal/mol, which proceeds according to direct H abstraction from $(\text{C}_2\text{H}_4)\text{Fe}^+\text{O}$ (**8**) followed by stepwise β-H shift with the highest barrier at –6.1 kcal/mol (see Fig S10, Supporting Information). Thus, loss of water is indeed a thermodynamically and kinetically favorable channel, which is different with the FTICR result ($\text{FeX}^+ < 12\%$ [20]). The difference can be rationalized by the fact that FeC_2H_2^+ could be quickly further oxidized to $\text{Fe}^+ + \text{C}_2\text{H}_2\text{O}$ by another N_2O due to the high reactivity of Fe^+ . This fact is supported by the efficient Fe^+ -catalyzed oxidation of C_2H_2 by N_2O , which has been studied in detail both experimentally and theoretically [31, 72]. Therefore, although C–C bond activation (FeCO^+) in the $\text{FeC}_2\text{H}_4^+ + \text{N}_2\text{O}$ reaction is kinetically unfavorable, the competing activation of C–H bond for producing FeC_2H_2^+ would decrease the selectivity of the O-atom transfer.

Formation of FeOH^+ and FeCH_2^+ is calculated to be endothermic by 8.2 and 2.1 kcal/mol, respectively (see Figs. S8 and S9, Supporting Information). However, as mentioned previously, owing to the overstability (~11 kcal/mol) of the $\text{FeC}_2\text{H}_4^+ + \text{N}_2\text{O}$ asymptote that should be taken into account, both two product channels would be really exothermic. Indeed, the exothermicities of

1.0 (−0.7) and 14.5 (12.8) kcal/mol for yielding FeOH^+ and FeCH_2^+ at 0 (298) K have been estimated through thermochemical calculations [73]. Note that except the $\text{FeC}_2\text{H}_4^+ + \text{N}_2\text{O}$ asymptote, the relative energies of the other dissociation channels are still described well at the present level of theory. Therefore, it is the high locations of the exit channels that explain the minor production of FeOH^+ and FeCH_2^+ , as observed in the experiment [20].

3.5 FeOH_2^+ oxidation by N_2O

The PES with the schematic structures involved is shown in Fig. 6. Information about the relevant species is given in Fig. S11 (Supporting Information). N_2O initially attaches to the metal of FeOH_2^+ forming $(\text{H}_2\text{O})\text{Fe}^+(\text{ON}_2)$ (**14**) and then is activated to yield $(\text{H}_2\text{O})\text{Fe}^+\text{O}(\text{N}_2)$ (**15**). The relevant ground barrier (${}^4\text{TS}_{14-15}$) lies at 7.0 kcal/mol above species **14** and 19.9 kcal/mol below ${}^6\text{FeOH}_2^+ + \text{N}_2\text{O}$, suggesting it should occur more readily, in comparison with the N_2O activation by FeC_2H_4^+ as described earlier. As shown in Fig. S11, ${}^4\text{TS}_{14-15}$ is featured by a cyc- $\text{Fe}^+-\text{O}-\text{N}^1$ structure, which favors formation of two singly occupied $\sigma(\text{Fe}^+\text{O})$ and $\sigma(\text{Fe}^+\text{N})$ orbitals, whereas for the analogous reaction with FeC_2H_4^+ , the metal center in ${}^4\text{TS}_{6-7}$ attaches at O from the end side of N_2O , forming only one singly occupied $\sigma(\text{Fe}^+\text{O})$ orbital. Thus, the O– N_2 activation by FeOH_2^+ favors an energetically lower-lying barrier in comparison with that by FeC_2H_4^+ .

Direct ejection of N_2 from **15** would account for the $(\text{H}_2\text{O})\text{FeO}^+$ oxide (**16**) ($E_{\text{rel}} = -52.5$ (46.2) kcal/mol for the sextet (quartet)), which could either release H_2O to form FeO^+ , or undergo direct O-to-O H shift yielding the energetically more stable complex $\text{Fe}(\text{OH})_2^+$ (**17**) ($E_{\text{rel}} = -66.9$ (−55.3) kcal/mol). The sextet (quartet) transition

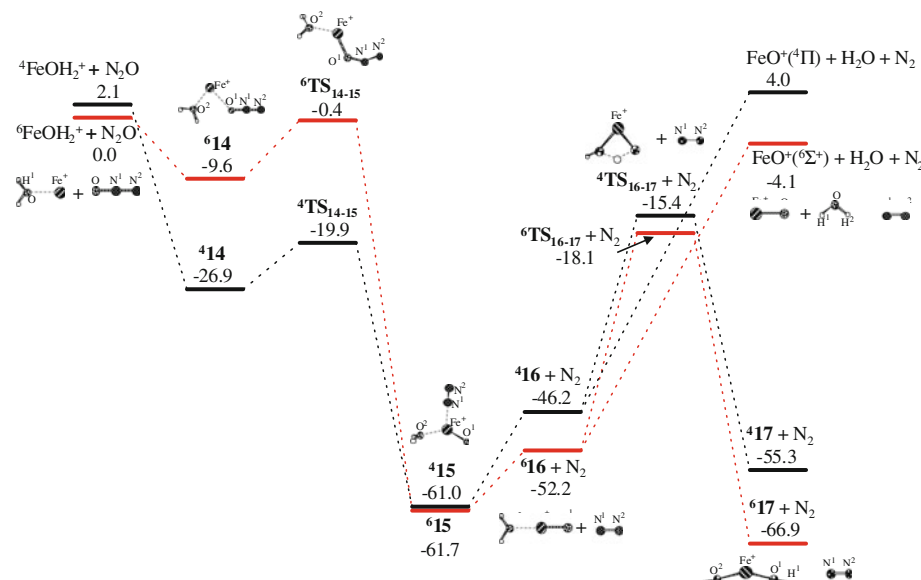
state (TS_{16-17}) for the H-shift is located at 18.1 (15.4) kcal/mol below the entrance channel and 14.0 (19.4) kcal/mol more stable than the exit channel of $\text{FeO}^+ + \text{H}_2\text{O}$ ($E_{\text{rel}} = -4.1$ (4.0) kcal/mol). Thus, the reactive FeO^+ regeneration is energetically unfavorable.

3.6 Gas-phase Fe^+ -mediated oxidation of C_2H_6 by N_2O

Gas-phase FTICR and collision-induced dissociation (CID) experiments have inferred that this reaction mainly produces $\text{C}_2\text{H}_5\text{OH}$, $\text{C}_2\text{H}_4\text{O}$, H_2O , and N_2 (reactions 1–4) [15, 20]. Owing to the formation of the $[\text{Fe}, \text{O}_2, \text{H}_2]^+$ as a side product, the turnover number for the reaction cycle is limited to about 2.5 [15, 20].

In the present theoretical investigation, after formation of FeO^+ via N_2O reduction by Fe^+ , ethane could be oxidized by the nascent oxide and partly converts via the C–O coupling mechanism to ethanol with 14.5 kcal/mol exothermicity. Also, it experiences an energetically more favorable β -H shift channel yielding water and ethylene, exothermic by 51.8 and 38.1 kcal/mol, respectively. This situation agrees with the CID and FTICR experimental findings, in which the $\text{H}_2\text{O}/\text{C}_2\text{H}_4/\text{C}_2\text{H}_5\text{OH}$ branching ratio was approximately determined to be 70: 20: 10 [15] (67: 21: 12 [20]). Note that the calculated exothermicities for losses of ethanol and ethylene match well with the experimental estimations by Schröder and Schwarz (14.5 vs. 13 and 38.1 vs. 31 kcal/mol) [20]. Furthermore, the calculated H_2O -loss exothermicity (51.8 kcal/mol) is much larger than that estimated by Schröder and Schwarz (36 kcal/mol [20]) but agrees well with that estimated by Jackson et al. (51 kcal/mol [15]).

Fig. 6 Energy profile for FeOH_2^+ oxidation by N_2O . Numbers refer to the relative stabilities (kcal/mol) with respect to the reactants of ${}^6\text{FeOH}_2^+ + \text{N}_2\text{O}$ evaluated at the B3LYP/DZVP(opt + 3f):6-311 + G(2d,2p) level including ZPE corrections. Scaling factor for the ZPE is 0.961



Another N_2O could react with the H_2O -loss partner FeC_2H_4^+ to yield $(\text{C}_2\text{H}_4)\text{Fe}^+\text{O}(\text{N}_2)$ (7). Due to the high barrier at -1.4 kcal/mol (see Fig. 3), the N–O activation forms the rate-determining step of the whole oxidation. The thermal $(\text{C}_2\text{H}_4)\text{Fe}^+\text{O}(\text{N}_2)$ would release a N_2 molecule and then is further oxidized to acetaldehyde, ethenol, and oxirane, regenerating Fe^+ (exothermic by 22.5, 10.9, and -7.5 kcal/mol, respectively). Carbonylation to acetaldehyde appears to be the most thermodynamically and kinetically favored channel as discussed previously.

The C_2H_4 -loss partner FeOH_2^+ could also reduce N_2O yielding $(\text{H}_2\text{O})\text{FeO}^+$. In comparison with C_2H_4 , the H_2O ligand is found to observably “enhance” the reactivity of Fe^+ toward N_2O , as mirrored by the O– N_2 activation barriers of 12.7, 20.9, and 7.0 kcal/mol with respect to the corresponding encounter complexes of Fe^+ON_2 , $(\text{C}_2\text{H}_4)\text{Fe}^+\text{ON}_2$, and $(\text{H}_2\text{O})\text{Fe}^+\text{ON}_2$, respectively. This fact is also supported by the FTICR experimental study, in which the corresponding rate constant k of the three reactions was determined to be 0.7×10^{-10} , 0.5×10^{-10} , and 6×10^{-10} $\text{cm}^3/\text{molecules}$, respectively, at room temperature [20]. However, $(\text{H}_2\text{O})\text{FeO}^+$ favors conversion into $\text{Fe}(\text{OH})_2^+$, rather than the reactive FeO^+ , explaining a low turnover number (about 2.5) of reaction cycles as observed in experiment [20].

4 Conclusions

The present theoretical work adds new insight into the gas-phase Fe^+ -mediated oxidation of ethane by N_2O . After initial N_2O reduction by Fe^+ yielding FeO^+ , ethane oxidation by FeO^+ as the second step of the reaction cycle involves initial C–H activation followed by two possible pathways, i.e., C–O coupling (for Fe^+ and ethanol), Fe^+ -mediated β -H shift (for the most energetically favorable products $\text{FeC}_2\text{H}_4^+ + \text{H}_2\text{O}$, with minor $\text{FeOH}_2^+ + \text{C}_2\text{H}_4$).

FeC_2H_4^+ reaction with another N_2O constitutes the third step of the oxidation. The initial O– N_2 activation by FeC_2H_4^+ to yield $(\text{C}_2\text{H}_4)\text{Fe}^+\text{O}(\text{N}_2)$ constitutes the rate-determining step of the whole oxidation. The thermal $(\text{C}_2\text{H}_4)\text{Fe}^+\text{O}(\text{N}_2)$ would release N_2 and then is further oxidized via a cyclization mechanism for yielding oxirane, acetaldehyde, and/or direct H-abstraction mechanism accounting for ethenol. The most favorable channel is the oxidation to acetaldehyde along the cyclization-C-to-C H-shift pathway. The C_2H_4 -loss partner FeOH_2^+ could rapidly react with N_2O to form $\text{Fe}(\text{OH})_2^+$, rather than the reactive FeO^+ .

Acknowledgments This work was supported by the Program for Changjiang Scholars and Innovative Research Team in University (IRT0759) of MOE, PRC, NSFC (21003158, 20476061, and

10979077), State Key Basic Research Program of China (2006CB202505), CNPC Science & Technology Innovation Foundation (2009D-5006-04-07), and Scientific Research Innovation Foundation of Graduate School of China University of Petroleum (SZ10-38).

References

- Shilov AE, Shul'pin GB (1997) *Chem Rev* 97:2879
- Torrent M, Solà M, Frenking G (2000) *Chem. Rev* 100:439
- Böhme DK, Schwarz H (2005) *Angew Chem Int Ed* 44:2336
- Schröder D, Schwarz H (1995) *Angew Chem Int Ed Engl* 34:1973
- Ueda W, Oshihara K (2000) *App Catal A* 200:135
- Solsona B, Vázquez MI, Ivars F, Dejoz A, Concepción P, López-Nieto JM (2007) *J Catal* 252:271
- Botella P, Dejoz A, Abello MC, Vázquez MI, Arrúa L, López-Nieto JM (2009) *Catal Today* 142:272
- Herreías CI, Yao XQ, Li ZP, Li CJ (2007) *Chem Rev* 107:2546
- Conley BL, Tenn WJ III, Young KJH, Ganesh SK, Meier SK, Ziatdinov VR, Mironov O, Oxgaard J, Gonzales J, Goddard WA III, Periana RA (2006) *J Mol. Catal A Chem* 251:8
- Periana RA, Mironov O, Taube D, Bhalla G, Jones CJ (2003) *Science* 301:814
- Roithvá J, Schröder D (2010) *Chem Rev* 110:1170
- Schröder D, Schwarz H (2007) *Top Organomet Chem* 1:1–22
- Eller K, Schwarz H (1991) *Chem Rev* 91:1121
- Irikura KK, Beauchamp JL (1989) *J Am Chem Soc* 111:75
- Jackson TC, Jacobson DB, Freiser BS (1984) *J Am Chem Soc* 106:1252
- Kang H, Beauchamp JL (1986) *J Am Chem Soc* 108:7502
- Kang H, Beauchamp JL (1986) *J. Am Chem Soc* 108:5663
- Ryan MF, Fiedler A, Schröder D, Schwarz H (1994) *Organometallics* 13:4072
- Lias SG, Bartmess JE, Liebmann JF, Holmes JL, Levin RD, Mallard WG (1988) *J Phys Chem Ref Data* 17:Suppl 1
- Schröder D, Schwarz H (1990) *Angew Chem Int Ed Engl* 29:1431
- Armentrout PB (2007) *Organometallics* 26:5486
- Holthausen MC, Koch W (1996) *J Am Chem Soc* 118:9932
- Holthausen MC, Fiedler A, Schwarz H, Koch W (1996) *J Phys Chem* 100:6236
- Zhang DJ, Liu CB, Bi SW, Yuan SL (2003) *Chem Eur J* 9:485
- Armentrout PB (2007) *Organometallics* 26:5473
- Yoshizawa K, Shiota Y, Yamabe T (1998) *J Am Chem Soc* 120:564
- Yoshizawa K, Shiota Y, Yamabe T (1999) *J Chem Phys* 111:538
- Shiota Y, Yoshizawa K (2000) *J Am Chem Soc* 122:12317
- Shiota Y, Yoshizawa KJ (2003) *Chem Phys* 118:5872
- Yoshizawa K, Shiota Y, Yamabe T (2000) *J Phys Chem A* 104:2552
- Zhao LM, Wang Y, Guo WY, Shan HH, Lu XQ, Yang TF (2008) *J Phys Chem A* 112:5676
- Liu ZC, Guo WY, Zhao LM, Shan HH (2010) *J Phys Chem A* 114:2701
- Zhao LM, Liu ZC, Guo WY, Lu XQ, Lin XQ, Shan HH (2008) *Chem Phys Lett* 463:54
- Zhao LM, Liu ZC, Guo WY, Zhang LZ, Zhang FY, Zhu HY, Shan HH (2009) *Phys Chem Chem Phys* 11:4219
- Yoshizawa K, Shiota Y, Yamabe T (1999) *J Am Chem Soc* 121:147
- Shiota Y, Suzuki K, Yoshizawa K (2005) *Organometallics* 24:3532

37. Harris N, Shaik S, Schröder D, Schwarz H (1999) *Helv Chim Acta* 82:1784
38. Shiota Y, Yoshizawa K (2001) *Organometallics* 20:1397
39. Engeser M, Schlangen M, Schröder D, Schwarz H (2003) *Organometallics* 22:3933
40. Schröder D, Holthausen MC, Kagawa Y, Schwarz H (2004) *J Phys Chem B* 108:14407
41. Feyel S, Schröder D, Rozanska X, Sauer J, Schwarz H (2006) *Angew Chem Int Ed Engl* 45:4677
42. Chen XX, Feng XS, Wang YC, Wang T, Liu XL, Zheng XW (2007) *Chem Phys Lett* 443:430
43. Rozanska X, Sauer J (2008) *J Int J Quantum Chem* 108:2223
44. Rozanska X, Sauer J (2009) *J Phys Chem A* 113:11586
45. Dietl N, Engeser M, Schwarz H (2009) *Angew Chem Int Ed* 48:4861
46. Scupp TM, Dudley TJ (2010) *J Phys Chem A* 114:1134
47. Schröder D, Schwarz H, Clemmer DE, Chen Y, Armentrout PB, Baranov VI, Böhme D (1997) *Int J Mass Spectrom Ion Process* 161:175
48. Frisch MJ, Trucks GW, Schlegel HB, Scuseria GE, Robb MA, Cheeseman JR, Montgomery Jr JA, Vreven T, Kudin KN, Burant JC, Millam JM, Iyengar SS, Tomasi J, Barone V, Mennucci B, Cossi M, Scalmani G, Rega N, Petersson GA, Nakatsuji H, Hada M, Ehara M, Toyota K, Fukuda R, Hasegawa J, Ishida M, Nakajima T, Honda Y, Kitao O, Nakai H, Klene M, Li X, Knox JE, Hratchian HP, Cross JB, Adamo C, Jaramillo J, Gomperts R, Stratmann RE, Yazyev O, Austin AJ, Cammi R, Pomelli C, Ochterski JW, Ayala PY, Morokuma K, Voth GA, Salvador P, Dannenberg JJ, Zakrzewski VG, Dapprich S, Daniels AD, Strain MC, Farkas O, Malick DK, Rabuck AD, Raghavachari K, Foresman JB, Ortiz JV, Cui Q, Baboul AG, Clifford S, Cioslowski J, Stefanov BB, Liu G, Liashenko A, Piskorz P, Komaromi I, Martin RL, Fox DJ, Keith T, Al-Laham MA, Peng CY, Nanayakkara A, Challacombe M, Gill PMW, Johnson B, Chen W, Wong MW, Gonzalez C, Pople JA (2003) Gaussian 03, revision B.05. Gaussian, Inc.: Pittsburgh, PA
49. Stephens PJ, Devlin FJ, Chabalowski CF, Frisch MJ (1994) *J Phys Chem* 98:11623
50. Becke AD (1993) *J Chem Phys* 98:5648
51. Lee C, Yang W, Parr RG (1988) *Phys Rev B* 37:785
52. Salahub DR (1989) The challenge of d and f electrons. In: Zerner MC (ed) ACS, Washington, DC
53. Parr RG, Yang W (1989) Density-functional theory of atoms and molecules. Oxford University Press, Oxford
54. Frisch MJ, Pople JA, Binkley JS (1984) *J Chem Phys* 80:3265
55. Chioldo S, Russo N, Sicilia E (2005) *J Comput Chem* 26:175
56. Seeger R, Pople JA (1977) *J Chem Phys* 66:3045
57. Bauernschmitt R, Ahlrichs R (1996) *J Chem Phys* 104:9047
58. Glendening ED, Reed AE, Carpenter JE, Weinhold F (1988) NBO Version 3.1
59. Reed AE, Curtiss LA, Weinhold F (1988) *Chem Rev* 88:899
60. Foster JP, Weinhold F (1980) *J Am Chem Soc* 102:7211
61. Freiser BS (ed) (1996) Organometallic ion chemistry. Kluwer, Dordrecht
62. Schultz RH, Armentrout PB (1993) *J Phys Chem* 97:596
63. Fiedler A, Schröder D, Schwarz H, Tjelta BL, Armentrout PA (1996) *J Am Chem Soc* 118:5047
64. Schultz RH, Crellin KC, Armentrout PB (1991) *J Am Chem Soc* 113:8590
65. Armentrout PB (2003) *Int J Mass Spectrom* 227:289
66. Tjelta BL, Walter D, Armentrout PB (2001) *Int J Mass Spectrom* 204:7
67. Sievers MR, Jarvis LM, Armentrout PB (1998) *J Am Chem Soc* 120:1891
68. Sugar J, Corliss C (1985) *J Phys Chem Ref Data* 14:1
69. Zhang DJ, Liu CB, Bian WS (2003) *J Mol Struct (Theochem)* 635:239
70. Schröder D, Schwarz H (1990) *Angew Chem Int Ed Engl* 29:1433
71. Roithova J, Schröder D (2007) *J Am Chem Soc* 129:15311
72. Kappes MM, Staley RH (1981) *J Am Chem Soc* 103:1286
73. On the basis of the following thermochemical data: $\Delta H_f^0(C_2H_4) = 12.5$ kcal/mol, $\Delta H_f^0(N_2O) = 19.61$ kcal/mol, $\Delta H_f^0(CH_2) = 92.45$ kcal/mol, $\Delta H_f^0(OH) = 9.32$ kcal/mol, $\Delta H_f^0(CH_2O) = -25.96$ kcal/mol ((1970) *Trans. Faraday Soc.* 66:794), $\Delta H_f^0(H_2CCH) = 71.5$ kcal/mol ((1996) Heats of Formation of Organic Free Radicals by Kinetic Methods in Energetics of Organic Free Radicals, Blackie Academic and Professional, London), $BDE(Fe^{+}-C_2H_4) = 35.0$ kcal/mol (ref 41), $BDE(Fe^{+}-CH_2) = 82.2$ kcal/mol (ref 39), and $BDE(Fe^{+}-OH) = 83$ kcal/mol (ref 37) at 298 K. Other data are from (1998) NIST-JANAF Thermochemical Tables, Fourth Edition, *J Phys Chem Ref Data*, Monograph 9, American Institute of Physics, New York